

Comparison between wind load by wind tunnel test and in-site measurement of long-span spatial structure

Hui Liu^{*1}, Wei-lian Qu¹ and Qiu-sheng Li²

¹*Hubei Key Laboratory of Roadway Bridge and Structure Engineering, Wuhan University of Technology, Wuhan, Hubei 430070, P. R. China*

²*Department of Building and Construction, City University of Hong Kong, Hong Kong, P. R. China*

(Received November 18, 2009, Accepted December 21, 2010)

Abstract. The full-scale measurements are compared with the wind tunnel test results for the long-span roof latticed spatial structure of Shenzhen Citizen Center. A direct comparison of model testing results to full-scale measurements is always desirable, not only in validating the experimental data and methods but also in providing better understanding of the physics such as Reynolds numbers and scale effects. Since the quantity and location of full-scale measurements points are different from those of the wind tunnel tests taps, the weighted proper orthogonal decomposition technique is applied to the wind pressure data obtained from the wind tunnel tests to generate a time history of wind load vector, then loads acted on all the internal nodes are obtained by interpolation technique. The nodal mean wind pressure coefficients, root-mean-square of wind pressure coefficients and wind pressure power spectrum are also calculated. The time and frequency domain characteristics of full-scale measurements wind load are analyzed based on filtered data-acquisitions. In the analysis, special attention is paid to the distributions of the mean wind pressure coefficients of center part of Shenzhen Citizen Center long-span roof spatial latticed structure. Furthermore, a brief discussion about difference between the wind pressure power spectrum from the wind tunnel experiments and that from the full-scale in-site measurements is compared. The result is important fundament of wind-induced dynamic response of long-span spatial latticed structures.

Keywords: long-span; spatial latticed structure; wind tunnel test; wind load; full-scale measurement.

1. Introduction

The subject of the study is a long-span spatial latticed structure. Due to the economic advantages and aesthetic appearance of spatial structures, these structures are now widely used for public buildings, sport arenas, exhibition centers, industrial factories, and so on. Since this type of spatial latticed structure is generally light and flexible, it tends to deflect and oscillate under turbulent wind forces. As the span increases, the natural frequencies generally decrease and the susceptibility of the roof to resonant excitation by turbulent wind action increases. Therefore, the wind effects on these long-span structures have some significant differences in comparison with those on the roofs of smaller low-rise buildings. Holmes (2001) indicated that the quasi-steady approach, although appropriate for small buildings, is not applicable for large roofs and resonant effects may be

* Corresponding Author, Dr., E-mail: drliuh@263.net

significant. Melbourne (1995) showed some resonant contributions to the responses of a large cantilevered roof. However, most codes and standards do not include the effects of resonant response on large roofs except the Australian Standard AS1170.2. There have been numerous wind tunnel studies on wind effects on long-span roofs (Holmes *et al.* 1997, 2001 and Melbourne 1995). However, to our best knowledge, comprehensive full-scale measurement of wind effects on extra-long-span spatial lattice structures such as Shenzhen Citizens Centre has not yet been reported.

Since the wind pressure on the long-span spatial latticed structure varies accordingly as time and space change, the time-space correlation of the pressure fluctuations may play an important role in its dynamic response. Although experimentally investigated the time-space correlation of the wind pressure in a wind tunnel, direct comparison of model testing results to full-scale measurements is always desirable, not only in validating the experimental data and methods but also in providing better understanding of the physics such as Reynolds numbers and scale effects. So, comparing model test results with actual performance is very useful. However, such comparison has rarely been made for long-span spatial structures under strong wind conditions.

The boundary layer wind tunnel (BLWT) is one of the great developments in structural engineering during the latter half of the last century. It has been the basic tool of wind engineering research on wind effects on buildings and structures, and most of the information in wind codes is based on wind tunnel testing and full-scale measurements. For example, the experimental tests were carried out in the BLWT for design of large roofs of the new Olympic stadium in Piraeus, Greece, and the wind tunnel data were used for the numerical simulation of the quasi-static response of the structure in the time domain, as it has been reported by Biagini *et al.* (2006, 2007). Characteristics of wind pressures on the large cantilevered roofs by BLWT were investigated by Zhao and Lam (2002). However, there are some problems involved with wind tunnel testing concerning wind effects on buildings and structures. For example, several wind tunnel measurements for the Texas Tech University Experimental Building (TTU Building) (Endo *et al.* 2006, Levitan *et al.* 1992 and Li *et al.* 1996) have been conducted and comparisons with full-scale measurements have been made. These wind tunnel measurements for different geometrical scale models all demonstrated a good agreement for mean pressure coefficients between wind tunnel tests and field measurements. However, fluctuating and negative peak pressure coefficients were significantly underestimated by a factor of one and a half to two in the model tests at the edge and roof corner locations for quartering winds. The reasons for causing the large discrepancies are not totally clear. Therefore, further comparisons between full-scale and model tests will be worthwhile, in particular, for a long-span structure such as Shenzhen Citizens Centre that is located in an area with a high incidence of typhoon winds. The field measurements of Shenzhen Citizens Centre can provide a fundamental improvement of knowledge in wind loading and response of long-span spatial structures.

Although there have been many advances in wind tunnel testing and numerical simulation techniques, many critical phenomena can still only be investigated by full-scale experiments. The most reliable evaluations of wind effects are obtained from experimental measurements of a prototype structure. Field measurements of wind effects on buildings and structures date back about 100 years. However, practical difficulties associated with operation and maintenance, and problems with instrumentation reliability led to many of the early field measurements being unreliable. Furthermore, very low frequency activity often introduces bias and non-stationarity into data records. During the last two decades, a revolution in data handling and collection has made enormous strides possible in full-scale measurements of wind effects on buildings and structures. Holmes (2001) and Jeary (1997) gave extensive literature reviews and detailed introductions on the

field measurements of wind effects on buildings and structures. Several tall buildings, including Di-Wang Tower with 325 m in height in Shenzhen and Gitic Plaza Hotel with 200 m in height in Guangzhou, Mainland China, and Central Plaza Tower with 374 m high and Bank of China Tower with 369 m in height in Hong Kong, in an attempt to investigate wind effects on tall buildings have been instrumented by the Q.S. Li *et al.* (1998, 2000, 2004, 2007). Therefore, wind pressures on the roofs have been evaluated rarely in the field measurement, only the experimental data obtained in a full-scale wind pressure study on the low-rise building, 3.3 m in height, located on the Loyola Campus of Concordia University in Montreal, Canada was reported by Stathopoulos *et al.* (1999).

An experimental campaign has been carried out in the BLWT at Shantou University, China (Fu *et al.* 2007), on the rigid model of the roof of Shenzhen Citizen Centre. The field measurements of Shenzhen Citizens Centre were executed by Wuhan University of technology, China (Qu *et al.* 2006). In order to compare the data-acquisition based on the BLWT experiment and based on in-site measurement, the weighted proper orthogonal decomposition (POD) technique is applied to the wind pressure data obtained from the non-uniformly distributed pressure taps in BLWT test since the location and quantity of the field measurement points of long-span roof does not coincide with those of the pressure taps on the roof model, wind-tunnel pressure data cannot be used directly in comparison with field measurement wind pressure data. Therefore, the pressure fluctuations at the roof spatial latticed structural nodes by applying a weighted POD technique to wind-tunnel pressure data. The POD analysis uncovers deterministic structures dominating on apparently random field. Armit first applied the POD in wind engineering to analyze wind pressure on a bluff body (1968). Best and Holmes investigated building wind loading using eigenvalues in the covariance integration method, which is an application of the POD described by Holmes and Best (1983). Bienkiewicz *et al.* (1995) applied the POD to analyze wind pressure on a low-rise building. Application of POD to simplify wind loads was discussed by Davenport (1995). The POD technique was applied in the analysis of the area-averaged fluctuating wind pressure on the roof of a low-rise building by Rocha *et al.* (2000). The POD was presented as simulation of wind pressure data by Tubino *et al.* (2007). The POD technique also was used to identify the loading mode and analyze the gust buffeting of long span bridges by double modal transformation Chen *et al.* (2006). The POD was extended also to include joint analysis of approach wind and building load reported by Tamura *et al.* (1995). In the many practical situations, pressure is acquired at locations that are not evenly spaced and a modified POD analysis is developed, a POD procedure appropriate for a case of pressure specified at non-uniformly distributed taps is proposed by Jeong *et al.* (1995). In the above studies, wind pressure is obtained in form of time history, however, structural response under wind-induced pressure is performed in the frequency domain, the wind pressure frequency domain characteristics is required. In the paper, a POD technique appropriate for pressure at non-uniformly distributions that can identify frequency domain characteristics of wind pressure is presented.

The present paper aims to obtain reliable field data that represent the real-time wind loading of the extra-long-span spatial structure. Measurements of data from the structure will include wind speeds, wind directions, and wind-induced pressures. The proposed field studies can provide us with very useful information on wind effects on long-span spatial structures. It also provides an excellent opportunity to use the full-scale measurements for correlation with theoretical and numerical models and comparison with wind tunnel test results. Particular attention has been given to the time and frequency characteristics of pressure measurement points including wind pressure time history, mean wind pressure coefficients, root-mean-square (rms) of wind pressure coefficient and wind pressure power spectrum and so on, and results have been compared with those of wind tunnel experiments.

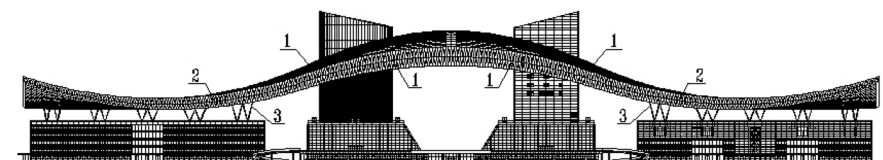
The study has provided useful insight into effect of extra-long-span spatial structure on the wind loadings.

2. Description of the long-span roof spatial latticed structure of Shenzhen Citizen Center

Shenzhen Citizens Centre, located in the central district of Shenzhen City, China, will be the new Shenzhen City Government Building and political pivot. It has about 210,000 square meters in gross building area. The whole building consists of tower groups in a central part along with eastern and western wings, as shown in Fig. 1. Two towers are located in the central part: one is a twelve-story circular-shaped tower with a diameter of a 36-meter; the other is a fifteen-story rectangular-shaped tower with a plan area of 36 mx45 m. The roof of Shenzhen Citizen Centre is of a spatial lattice structure supported by tree-shaped steel columns and with the two towers underneath. The roof is 486 meters long, and its width changes from 120 m in the central part to 154 m at its two ends, while its depth varies from 2.25 m to 9.00 m. The height from ground to top of the roof is 80 m. To the best knowledge of the applicants, the roof structure of Shenzhen Citizens Centre is the longest spatial lattice structure in the world. The upper and lower surfaces of the roof are all curve shaped, and the lower surface is covered with roof panels having 13.6% hollow area. The whole roof consists of three parts: one central part and two symmetric wings. The two symmetric wings have a double-layer tetrahedral spatial lattice structure with bolt-connected ball joints, supported by 17 tree-shaped columns. The rods of spatial lattices are circular steel tubes, and the connections between the rods are bolt-connected ball joints. The central part of the roof is a compound space structural system that consists of three subsystems: (1) main trusses around the circular-shaped tower and rectangular- shaped tower; (2) spatial lattices between the main trusses; (3) spatial lattices connected to the main trusses and the tree-shaped supports at its two ends. A welded box type section is



(a) Picture of Shenzhen Citizen Center



1 main truss, 2 structural joint 3 tree-shaped columns

(b) Elevation view

Fig. 1 Overview of Shenzhen Citizen Center

adopted in the main trusses, while the spatial lattice is of three-layer tetrahedral space truss structure with welded hollow ball joints. The spatial lattices are connected with the main trusses by semi-ball joints with ribs.

The distribution of wind pressures on the center part of the roof is very complicated; and the brace span of center part of spatial latticed structure is long and its brace system is less than other parts. Therefore, it is chose as object of filed measurement wind pressure.

3. Experimental works

3.1 Full-scale measurements

The field measurements are carried out on the center part of long-span spatial latticed structure of Shenzhen Citizen Center in Shenzhen city, Guangdong province, China. For measuring pressure, the wind pressure sensors with measurement range from -10 Kpa to 10 Kpa are used, whose distribution required for experiment is illustrated in Fig. 2. Fig. 2 shows the center part of roof, which is a curve roof, 268 m long, 130 m wide, and these 20 pairs wind pressure sensors are installed around the same locations on both the upper and lower roof surfaces.

For the measurement of wind speed and direction, a wireless anemometer is placed on a mast mounted on the Shenzhen Citizen Center plaza to avoid wind interference with the flow passing over the structure. The height of anemometer is 7 meters. The wind direction is defined as angle from the east along an anti-clockwise direction and varied from 0° to 360° with incremental step of 15°, there are 24 wind directions.

Data collection will only be started automatically when the control computer is starting up. Full-scale pressure measurements executed by using transform unit, synchronous card and A/D card with sampling rate 25 Hz. Data are subsequently transferred to the control computer for mass storage and further analysis, and the results are stored in database. A typical record of data collected consists of 15000 samples in every 10 minutes duration. The wind pressure coefficient $C_{pi}^m(t)$ at wind pressure sensor i values are wind pressures $p_i(t)$ referenced to the mean dynamic velocity pressure.

$$C_{pi}^m(t) = \frac{p_i(t)}{1/2\rho V^2} \tag{1}$$

Here ρ is density of air. V is the 10-min mean velocity at the roof height for records which are

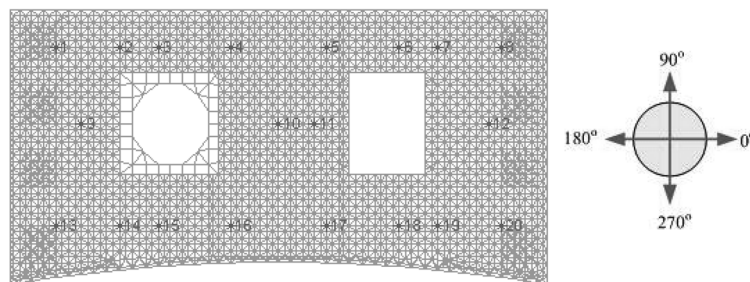


Fig. 2 Layout and serial number of the wind pressure sensors

stationary as far as the wind direction is concerned, assuring that the wind direction has not fluctuated beyond the range of 15° during this period. Furthermore, the standard variance and wind pressure power spectrum of the wind pressure record are analyzed.

3.2 Wind-tunnel measurement

Wind tunnel experiments were carried out in the BLWT at Shantou University. The wind tunnel has working section 3 m wide × 2 m high and 20 m long. A rigid model with a geometric length scale of 1:400 was made to represent the Shenzhen Citizen Centre. The photograph of the model mounted in the wind tunnel is shown in Fig. 3. Spires and roughness elements were used to simulate a typical boundary layer wind flow stipulated in the Load Code of China (2002) as exposure category C. This terrain type specifies a mean wind speed profile with a power law exponent of $\alpha = 0.22$ and a gradient height of 400 m. The spectrum of longitudinal wind speed at height of 90 m (0.225 m above the wind tunnel test section) is in good agreement with the von Karman type spectrum (Fu *et al.* 2007).

The upper and lower surfaces of the roof of Shenzhen Citizen Centre are exposed to wind actions. Therefore, in order to obtain the pressure differences between both sides of the roof, 348 pairs of pressure taps were installed at the same locations on both the upper and lower roof surfaces, which are marked with as shown in Fig. 4, for the pressure measurements. The layout of the pressure taps on both the upper and lower roof surfaces is shown in Fig. 4. The wind direction is defined as same

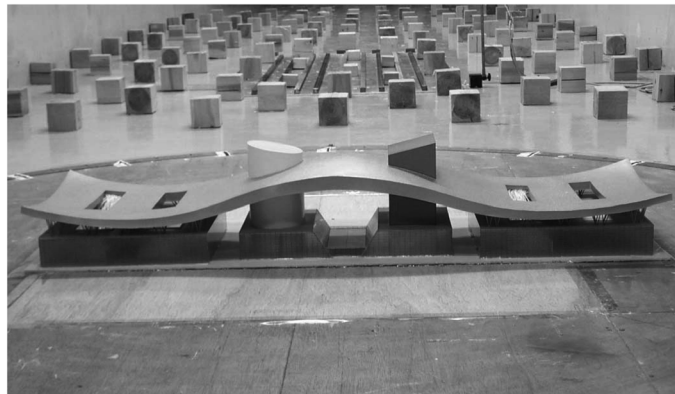


Fig. 3 The model of Shenzhen Citizen Center in the wind tunnel test

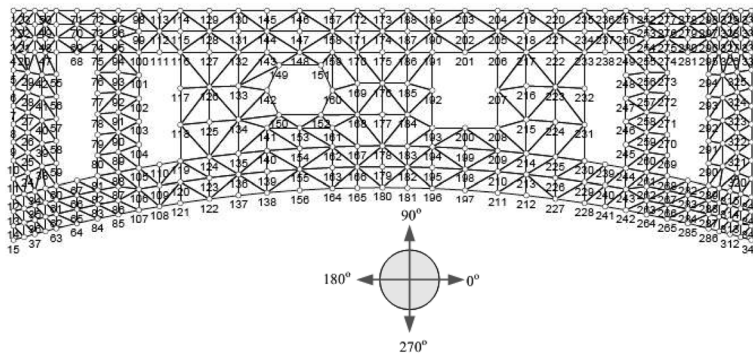


Fig. 4 Layout and serial number of the pressure taps

as full-scale measurements.

The pressure measurements were executed at a wind velocity of 7.5 m/s at a reference height 60 cm in the wind tunnel tests. The wind pressure coefficient $C_{pj}^e(t)$ of the pressure tap j on the roof due to the combined action of the pressures on the upper and lower roof surfaces is determined as follows

$$C_{pj}^e(t) = \frac{P_{uj}(t) - p_{lj}(t)}{p_0 - p_\infty} \quad (2)$$

Here $p_{uj}(t)$ and $p_{lj}(t)$ are the measured upper and lower surface pressures at the tap j , respectively. p_0 and p_∞ are the total pressure and the static pressure at the reference height, respectively. The results of wind tunnel tests were reported by Fu and Li (2007).

3.3 Experimental comparison results

The experimental results for the full-scale center part roof are compared with those for wind tunnel model tests and full-scale studied to verify the proper work of the instrumentation. However, the positions of the pressure taps on the wind tunnel model don't coincide with those of the wind pressure sensors on the full-scale center part roof, and the quantity of the wind pressure sensors is less than it of the pressure taps on the wind tunnel model. In order to accomplish comparison between the wind pressure by wind tunnel experiment and that by full-scale measurement, the weighted POD technique is applied to the wind pressure data obtained from the non-uniformly distributed pressure taps in BLWT tests. Since the locations of wind pressure sensors on the full-scale center part roof are determined by the finite element model nodes' locations of center part roof latticed structure, therefore, wind pressure fluctuations are simulated at the structural nodes by applying the weighted POD technique to the wind tunnel pressure data; the wind pressure fluctuations on the locations of wind pressure sensors are obtained based on the wind tunnel tests.

Following the POD approach, consider the random pressure filed $P(x_i, y_j, t)$ at time t , and position $(x_i, y_j)(i, j = 1, 2, \dots, n)$. From the wind pressure time series, the mean vector and covariance matrix $[R]$ are estimated. When the roof spatial latticed structure is applied to uniformly distributed wind pressure taps in the wind tunnel tests, the weighting $[W]$ is utilized that is a tributary area associated with each wind pressure taps. Then

$$[R][W]\{\Phi\}_k = \lambda_k\{\Phi\}_k \quad (3)$$

Where, λ_k is the eigenvalue of the covariance matrix associated with eigenvector $\{\Phi\}_k$, $k = 1, 2, \dots, n$, and n is the quantity of wind pressure taps. To ensure real eigenvalues and orthogonal eigenvectors in solution of a discrete eigenvalue problem, it is necessary to keep the matrix Hermitian. $[R^w] = [W]^{1/2}[R][W]^{1/2}$ is introduced

$$[R^w]\{\Phi^w\}_k = \lambda_k^w\{\Phi^w\}_k \quad (4)$$

It can be proven that the matrices $[R^w]$ and $[R]$ have the same characteristic polynomial, and thus they have the same eigenvalues. The sought eigenvectors $\{\Phi\}_k$ can be recovered from

$$\{\Phi\}_k = [W]^{-1/2} \{\Phi^w\}_k \quad (5)$$

The wind pressure at time t may be expressed by the following equation,

$$P(x_i, y_j, t) = \sum_{k=1}^n a_k(t) \varphi_k(x_i, y_j) \quad (6)$$

Here $\|\{\Phi\}_i\| = 1, i = 1, 2, \dots, n$ and $\{\Phi\}_i^T \{\Phi\}_j = 0, (i \neq j)$. The coefficients $a_k(t), k = 1, 2, \dots, n$, are zero mean, uncorrelated random variables with variance of a_k equal to the eigenvalue of the covariance matrix associated with eigenvector $\{\Phi\}_k$. It can be calculated as follows

$$a_k(t) = \frac{\sum_i^n \sum_j^n P(x_i, y_j, t) \varphi_k(x_i, y_j)}{\sum_i^n \sum_j^n \varphi_k^2(x_i, y_j)} \quad (7)$$

The eigenvalue λ_k is the measure of the contribution of each eigenmode to the wind pressure mean squares. It is normalized as follows

$$P_k = \frac{\lambda_k}{\sum_{j=1}^n \lambda_j} \quad (8)$$

According to the normalized eigenvalues P_k , the span of the modes used in the reduced-order model describes the reduced-order subspace of the POD model. The wind pressure is described by the reduced-order POD model in this lower-dimensional subspace.

$$\{P\} = [\Phi] \{a\} \quad (9)$$

Where the dimension of $[\Phi]$ is $n \times m$, $m < n$ is only the first m main eigenmodes of pulsation wind pressure are reserved. The values of eigenvectors ($\{\bar{\Phi}\}_k$) $_{N \times 1}$ of pulsation wind pressure at structural nodes are interpolated and extrapolated from those at measurement point's locations, N is the quantity of roof structural nodes.

$$\{\bar{P}(t)\}_{N \times 1} = [\bar{\Phi}]_{N \times m} \{a\}_{m \times 1} \quad (10)$$

Where $\{a\}$ is $m \times 1$ vector, according to the relationship pulsation wind pressure vector and vector $\{a\}$, the power spectral density function matrix can be denoted,

$$[S_{\bar{P}}]_{N \times N} = [\bar{\Phi}]_{N \times m} [S_a]_{m \times m} [\bar{\Phi}]_{m \times N}^T \quad (11)$$

Applied to covariance matrix of pulsation wind pressure on the pressure taps, power spectral density function matrix of pulsation wind pressure can be identified which can be denoted as power

spectral density function matrix $[S_a]$ of the low-dimension random process vector $\{a\}_{m \times 1} (m \ll N)$.

3.3.1 Wind pressure time history

In the wind tunnel tests, the design wind speed with 100 years return period for Shenzhen city is 61.1 m/s at a height of 240 m according to the Load Code for the Design of Building Structures in China. Therefore, the velocity scale in the wind tunnel tests is approximately 1/8.1 and time scale is 1/49. Furthermore, the sampling frequency and record length in the wind pressure measurements are equivalent to 6.38 Hz and 53.5 minutes in full-scale respectively. The period for analyzing the wind pressure fluctuations is taken to be 10 minutes, which is the same as the period of full-scale measurements and is usually used as the average time in wind speed or pressure measurements in China.

The present full-scale results at wind direction 75° and wind speed 2.26 m/s at the height of 7 m are available; Fig. 5 shows the wind pressure time history for sensors 3, 12 and 16 in full-scale in-site measurements. Fig. 6 shows the wind pressure time record for the same location as sensors 3, 12 and 16 based on the weighted POD technique in wind tunnel tests at wind direction 75° . Note

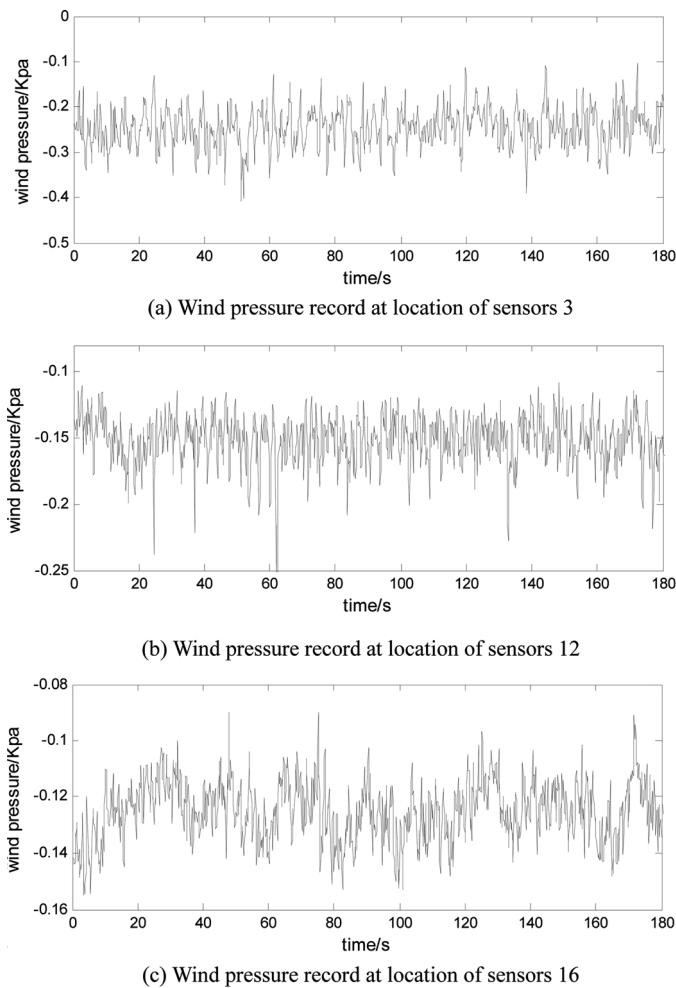
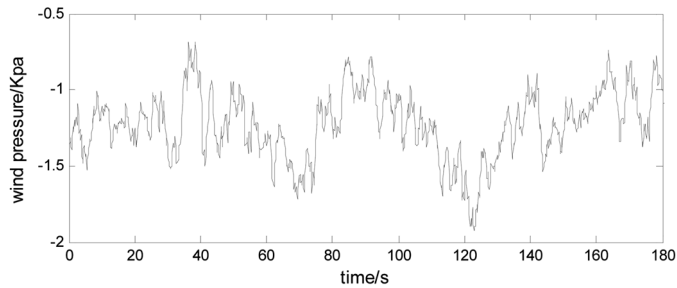
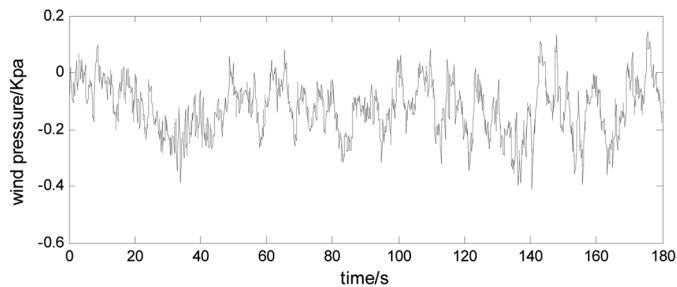


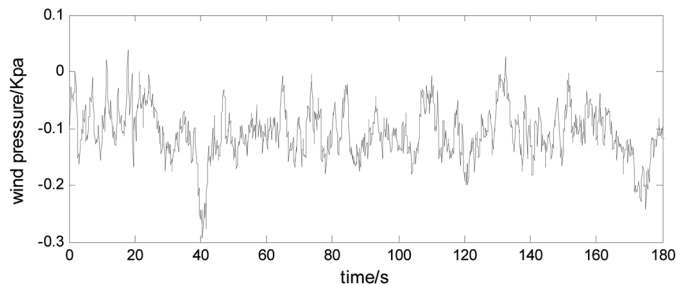
Fig. 5 Wind pressure record in full-scale measurements on wind direction 75°



(a) Wind pressure record at location of sensors 3



(b) Wind pressure record at location of sensors 12



(c) Wind pressure record at location of sensors 16

Fig. 6 Wind pressure record in wind tunnel tests on wind direction 75°

that all these data from wind tunnel tests and full-scale measurements are dominated by negative, it illustrates that wind pressures represent suction on the center part roof at wind direction 75° . The statistics of pressure fluctuations of 20 sensors locations from wind tunnel tests and full-scale measurements including minimum, maximum and mean of wind pressure are listed as Table 1. The case 1 and case 2 in Table 1 represent statistics of pressure fluctuations from wind tunnel tests and full-scale measurements respectively. The mean wind pressure, maximum wind pressure and minimum wind pressure comparison results on the location of wind pressure sensors are shown as Figs. 7, 8 and 9 respectively. The data show that, mean wind pressures exhibit highest at sensor 15 and lowest at sensor 1 in full-scale measurement results, as well as exhibit highest at sensor 16 and lowest at sensor 3 in wind tunnel experiment results; maximum wind pressures exhibit highest at

Table 1 The comparison of Maximum, Minimum and Mean wind pressure by wind tunnel tests and full-scale measurements (Case 1 = wind tunnel tests, case 2 = full-scale measurements)

Locations of sensors	Maximum of wind pressure (Kpa)		Minimum of wind pressure (Kpa)		Mean of wind pressure (Kpa)	
	Case1	Case2	Case1	Case2	Case1	Case2
1	-0.3003	-0.1833	-1.406	-0.3745	-0.8279	-0.2714
2	-0.5875	-0.0601	-1.543	-0.3759	-1.013	-0.2211
3	-0.6587	-0.0988	-1.924	-0.4106	-1.228	-0.2455
4	-0.0765	-0.0456	-1.341	-0.2269	-0.7141	-0.1248
5	-0.1217	-0.0131	-1.281	-0.3088	-0.7338	-0.1268
6	0.3010	-0.0922	-1.253	-0.3852	-0.4432	-0.1811
7	0.7190	-0.0017	-1.136	-0.4039	-0.3173	-0.1873
8	0.1905	-0.1754	-1.076	-0.3938	-0.4625	-0.2688
9	-0.0877	-0.0313	-0.5764	-0.2563	-0.2880	-0.1646
10	-0.1526	-0.1612	-0.8999	-0.2747	-0.5092	-0.2087
11	-0.3211	-0.1644	-0.9909	-0.3317	-0.5839	-0.2350
12	0.2506	-0.1010	-0.5032	-0.2971	-0.1281	-0.1517
13	0.0823	-0.0172	-0.4624	-0.1982	-0.1783	-0.1080
14	0.0017	0.0	-0.3584	-0.2080	-0.1824	-0.1144
15	0.0814	-0.0397	-0.3091	-0.1176	-0.1196	-0.0813
16	0.0375	-0.0897	-0.2932	-0.1627	-0.1107	-0.1263
17	0.0372	-0.0693	-0.5795	-0.1560	-0.2701	-0.1143
18	0.1972	-0.0625	-0.4667	-0.2004	-0.1433	-0.1262
19	-0.1052	-0.0674	-0.7895	-0.2726	-0.3580	-0.1305
20	-0.0880	-0.0619	-0.4337	-0.1424	-0.2532	-0.1041

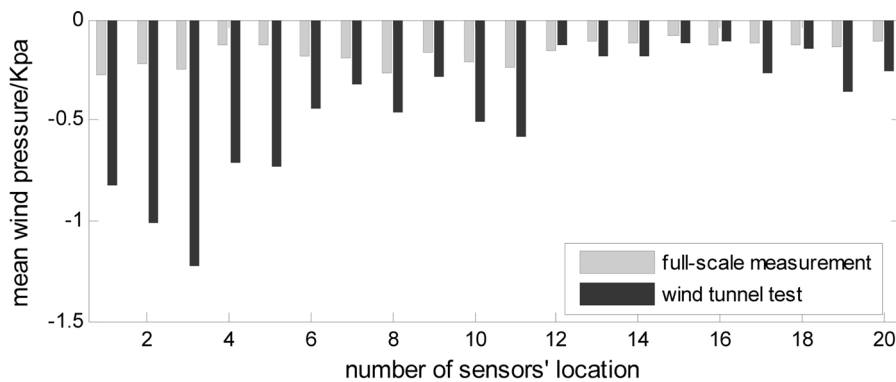


Fig. 7 The comparison of mean wind pressure between wind tunnel tests and full-scale measurements

sensor 6 and lowest at sensors 1 in full-scale measurement results, as well as exhibit highest at sensor 7 and lowest at sensor 3 in wind tunnel experiment results; minimum wind pressures exhibit

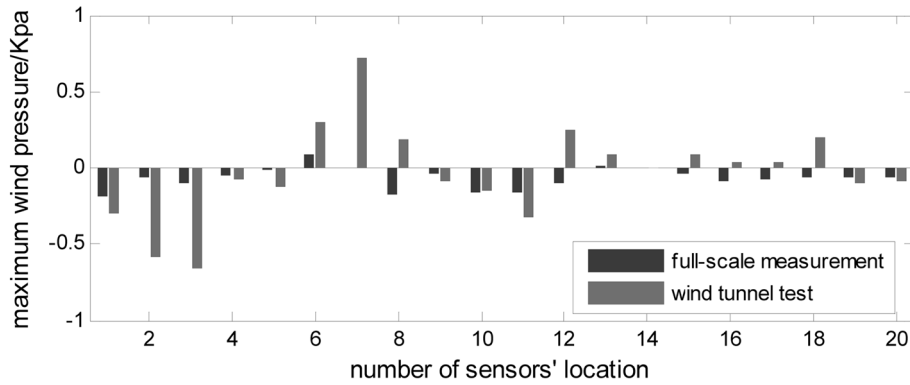


Fig. 8 The comparison of maximum wind pressure between wind tunnel tests and full-scale measurements

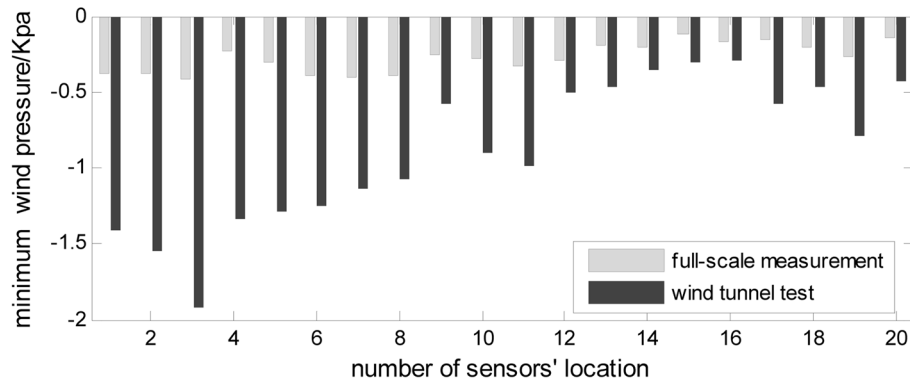


Fig. 9 The comparison of minimum wind pressure between wind tunnel tests and full-scale measurements

highest at sensor 15 and lowest at sensor 3 in full-scale measurement results, as well as exhibit highest at sensors 16 and lowest at sensor 3 in wind tunnel experiment results. Although the minimum wind pressures exhibit lowest at sensor 3 in the full-scale measurement results which is same as it in the wind tunnel test results, there are deviation of location which another extreme values appear comparison between full-scale measurement results and wind tunnel test results. From Fig. 2, the location of sensor 15 is adjacent to the location of sensor 16, and the location of sensor 6 is adjacent the location of sensor 7, only the location of sensor 1 is a little far away from the location of sensor 3, whereas, the extreme values' orientation of mean wind pressure, maximum wind pressure and minimum wind pressure are approximately the same between the full-scale measurement results and the wind tunnel experiment results. The data of wind direction 75° from the full-scale measurements and the wind tunnel tests are rather good agreement.

3.3.2 Mean wind pressure coefficient

In the wind tunnel tests, the mean wind pressure coefficients are obtained by Eq. (2). Fig. 10 shows the distribution of the mean wind pressure coefficients on the center part of the roof at the wind direction 75° . The roof surfaces are mainly under suction pressure, in particular relatively high negative pressure coefficients occurring near the leading edges. High negative pressure region is limited to the areas near the windward roof edges; and in other regions the spatial variation and the

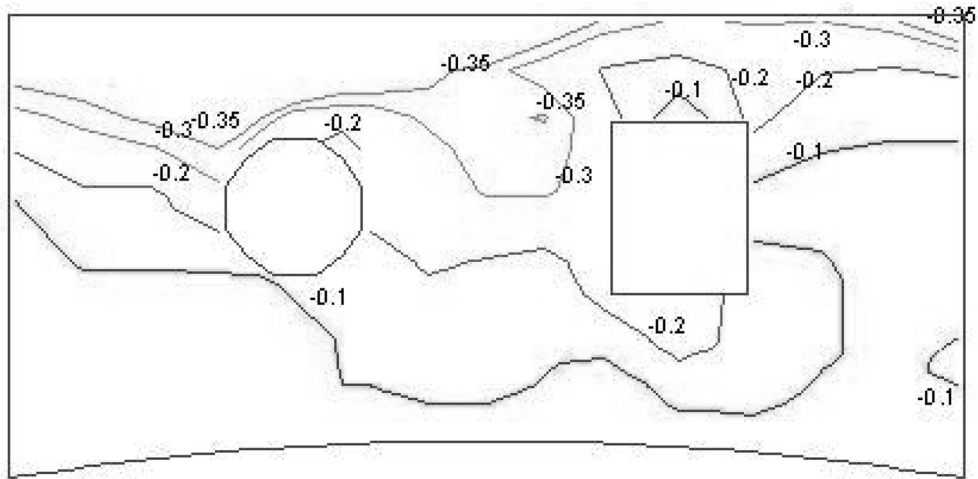


Fig. 10 Mean pressure coefficient distributions on the center part of roof in wind tunnel tests on wind direction 75°

magnitude of mean wind pressure coefficient is fairly small.

In the full-scale measurements, the mean wind pressure coefficients are obtained by Eq. (1). Fig. 11 shows the mean wind pressure coefficients comparison of the data for 20 sensors' locations between the wind tunnel test results and full-scale measurement results. The data show that mean wind pressure coefficients exhibit highest value at sensor 15 and lowest value at sensors 1 in full-scale measurement results, as well as exhibit highest value at sensors 16 and lowest value at sensor 3 in wind tunnel experiment results, minimum and maximum wind pressure coefficients are found on the approximate region between the wind tunnel results and full-scale measurement results. The high negative pressure region appeared near the windward roof edges from the wind tunnel test results and full-scale measurement results. Data indicate that in general all wind pressure sensors exhibit high suction for oblique incident winds of 75° , similar trends have been noticed in the wind tunnel and in full scale.

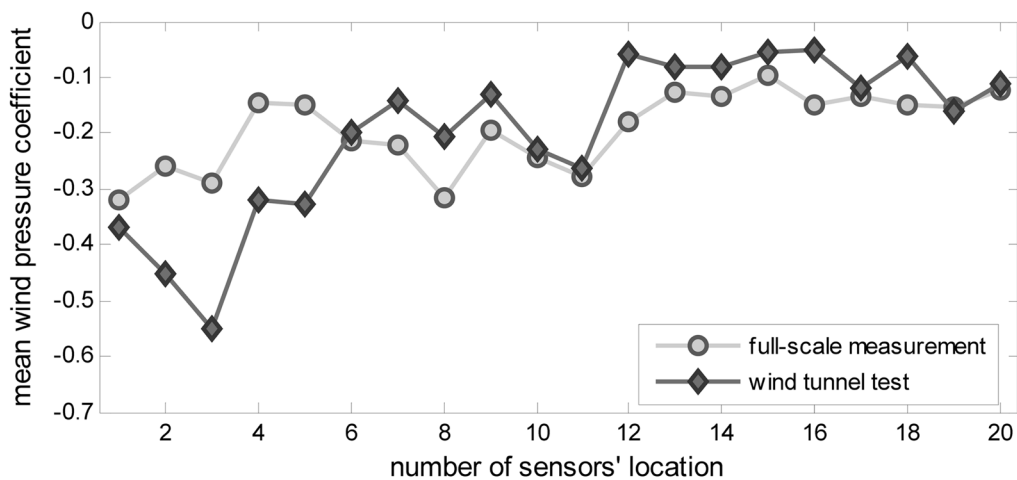


Fig. 11 The comparison of mean wind pressure coefficients on wind direction 75°

3.3.3 Root-mean-square of wind pressure coefficient

The contour of rms of wind pressure coefficient distributions is plotted in Fig. 12 for the wind direction 75° based on the wind tunnel test. It can be seen from Fig. 12 that the worst rms of wind pressure coefficient of 0.35 occur at the windward of the center part of roof and its magnitude decrease from 0.35 to 0.15 from the leading edges to the rear edges on the center part of the roof.

Fig. 13 compares the rms of wind pressure coefficient obtained for 20 wind pressure sensors' locations in full-scale and in the wind tunnel for the center part of the roof. It should be mentioned that the high rms of wind pressure coefficient occur at windward corners of center part of the roof from the wind tunnel test results and full-scale measurement results. The rms of wind pressure coefficient for full-scale measurement results is smaller than that for wind tunnel test results, whereas data indicate that similar trend of rms of wind pressure coefficient in the wind tunnel and in full scale.

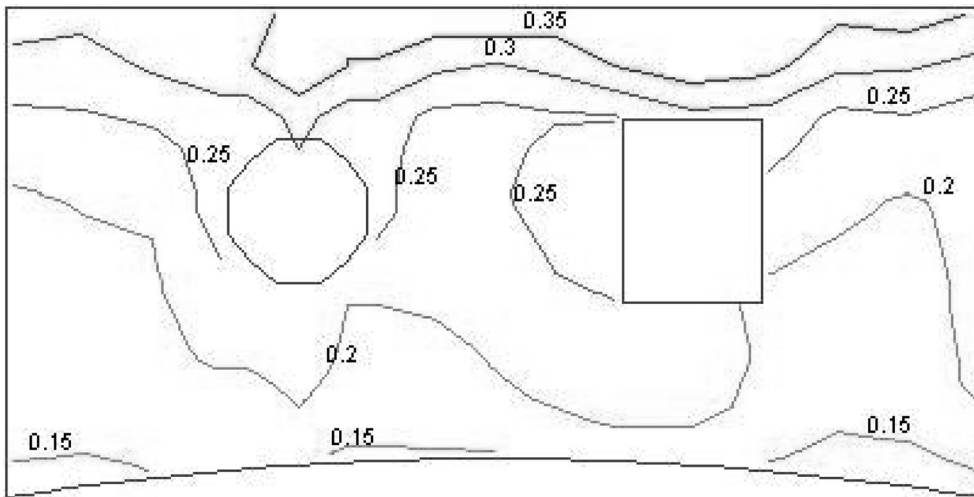


Fig. 12 Root-mean-square pressure coefficient distributions on center part of the roof in wind tunnel tests on wind direction 75°

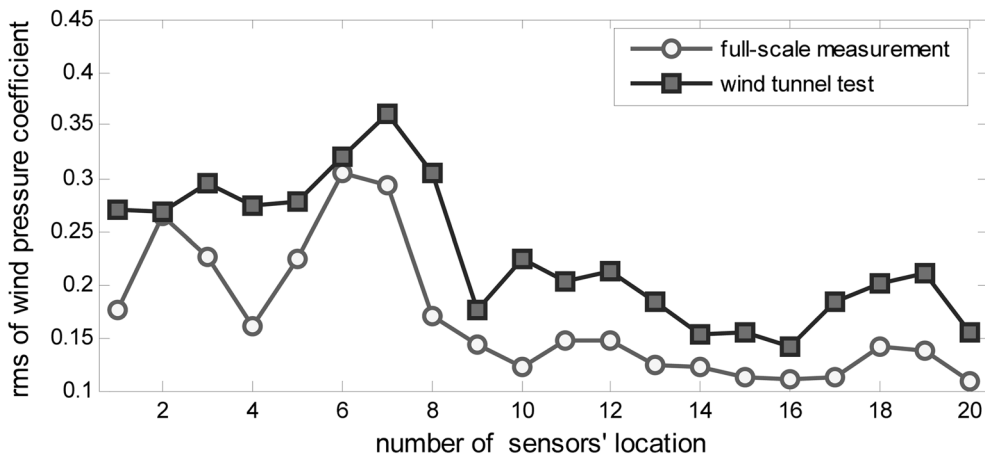


Fig. 13 The comparison of rms of the wind pressure coefficient on wind direction 75°

3.3.4 Wind pressure power spectrum

The in-site measured wind pressure power spectrum of the center part of the roof is compared with that obtained by the wind tunnel tests on wind direction 75° . Since some measurement noise is mixed with the full-scale measurement results, the filter that is provided by MATLAB is utilized to eliminate measurement noise influence. The filter function filters a data sequence using a digital filter which works for inputs; it is a direct form II transposed implementation of the standard difference equation. The comparison results for after and before filter at sensors 10 are shown in Fig. 14, it indicated that the power spectrum curve of wind pressure after filter is smoother than it before filter, and measurement noise influence is reduced.

Figs. 15, 16 and 17 compare the wind pressure power spectrum obtained for sensors 3, 12 and 16 in full scale and wind tunnel for the center part of the roof. It should be mentioned that the shape of the wind pressure power spectrum at sensor 3 is a little different between wind tunnel test results and full-scale measurement results; it may be caused by measurement environment factors. The shape of wind pressure power spectrums for sensors 12 and 16 agrees with full-scale data as compared to wind tunnel test data.

4. Conclusions

The wind pressure characteristics on long-span roof of Shenzhen Citizen Center were investigated by wind tunnel tests, furthermore, wind pressure measurements were carried out in full scale and the results for the full-scale roof were compared with wind tunnel results. The wind pressure time history, mean wind pressure coefficient, wind pressure rms and wind pressure power spectrum were studied based on wind tunnel tests and full-scale measurement. Conclusions from the comparison between wind tunnel measurement results and full-scale measurement results study are summarized,

1. The center part roof of Shenzhen Citizen Center was dominated by negative wind pressure, and the high negative pressure occurred near the windward roof edges from the wind tunnel test results

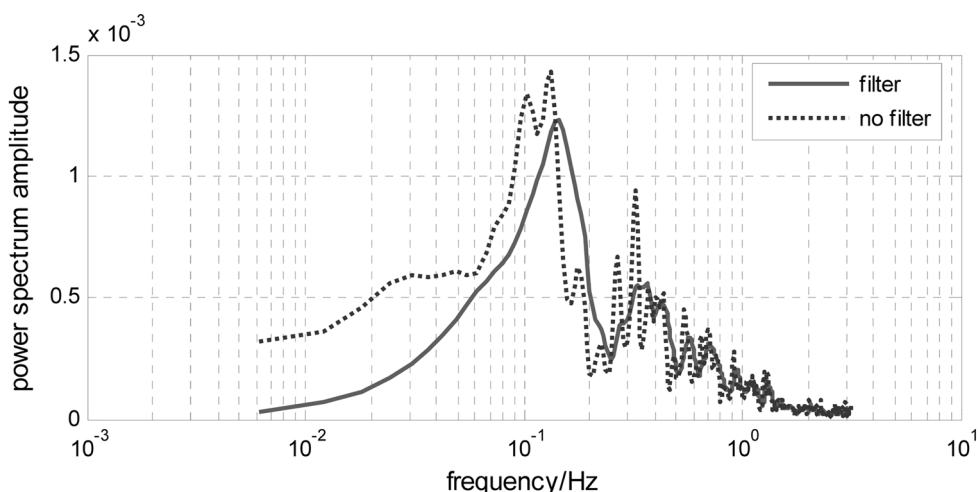


Fig. 14 The comparison of wind pressure power spectrum for before and after filter at sensor10

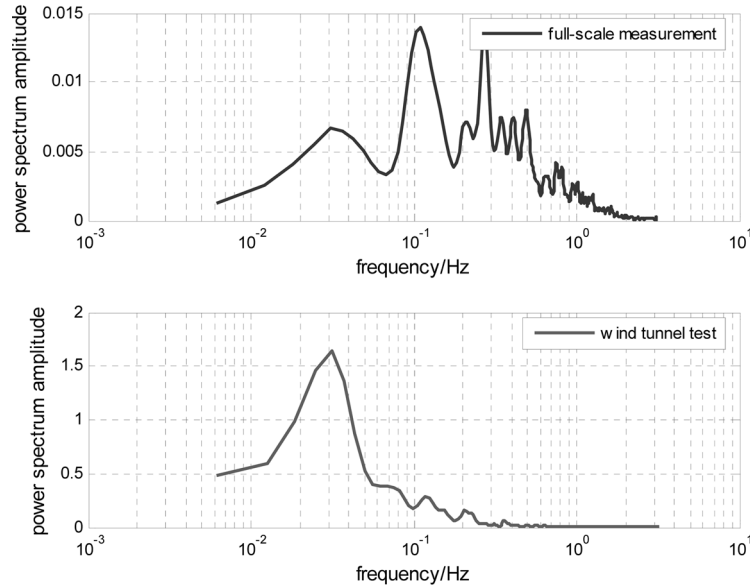


Fig. 15 The comparison of wind pressure power spectrum in full scale and wind tunnel at sensor 3

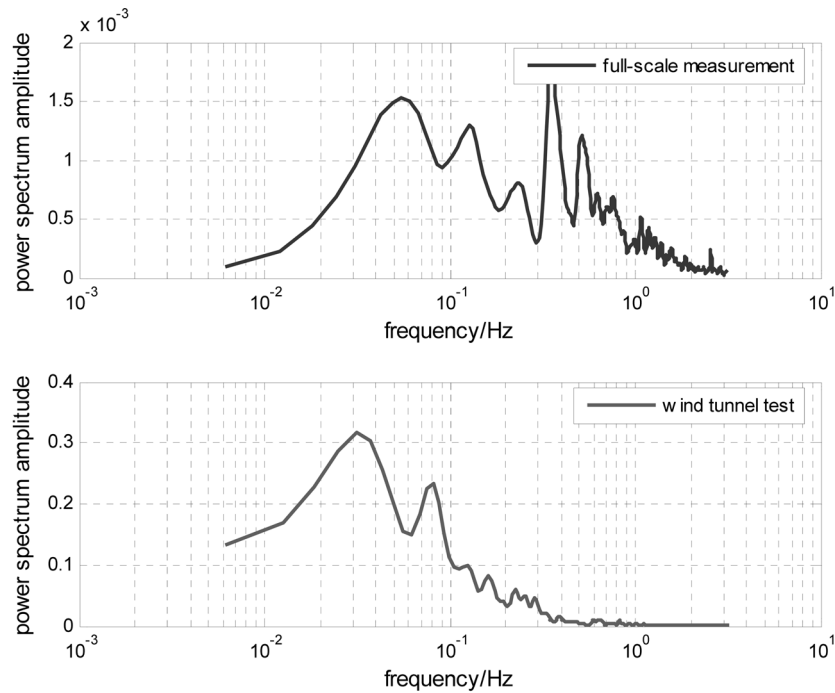


Fig. 16 The comparison of wind pressure power spectrum in full scale and wind tunnel at sensor 12

and full-scale measurement results. Larger and smaller magnitudes of the mean pressure coefficients were measured at near locations by comparison between the wind tunnel tests and full-scale measurements. Moreover, for wind pressure similar trends have been noticed in the wind tunnel and

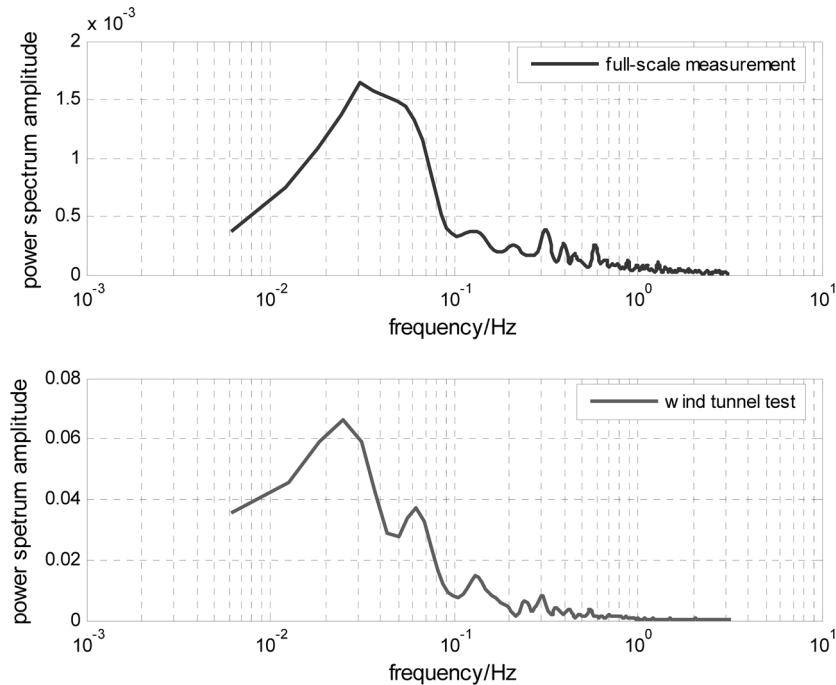


Fig. 17 The comparison of wind pressure power spectrum in full scale and wind tunnel at sensor 16

in full scale. A majority of mean wind pressures coefficients by wind tunnel tests are proximity those by full-scale measurements.

2. The distribution characteristics of wind pressure coefficients rms were similar to those of mean wind pressure coefficients, the high magnitude of wind pressure coefficients rms occurred near the windward roof edges. The rms of wind pressure coefficients for full-scale measurement results are smaller than those for wind tunnel test results, whereas there are similar trend of rms of wind pressure coefficients in the wind tunnel and in full scale.

3. The wind pressure power spectrum comparison between the wind tunnel tests results and the full-scale measurements results was accomplished, the a majority of shapes of wind pressure power spectrum based on the wind tunnel tests agree with those based on the full-scale measurements.

The comparison results indicated that distributions and trends of wind pressure by wind tunnel tests were analogical to those by the full-scale measurements mostly. The deviation cause of the comparison results was difference measurements environments; the full-scale measurements environment was more severe. Furthermore, the roof of Shenzhen Citizen Center was not exposure standard category C, it is located where was only close to the category C site. The simulation wind environment of wind tunnel was the approximate to the real wind environment.

Acknowledgements

Financial support of this work provided by a grant from the Chinese National Science Foundation (Project No.: 51078301, 50830203) and the Research Grants Council of Hong Kong Special

Administrative Region, China (Project No.: CityU 1266/03E) are gratefully acknowledged.

References

- Armitt, J. (1968), "Eigenvector analysis of pressure fluctuations on the West Burton instrumented cooling tower", Internal Report RD/L/N/ 114/68, Central Electricity Research Laboratories (UK).
- Best, R.J. and Holmes, J.D. (1983), "Use of eigenvalues in the covariance integration method for determination of wind load effects", *J. Wind Eng. Ind. Aerod.*, **13**(1-3), 359-370.
- Biagini, P., Borri, C. and Facchini, L. (2007), "Wind response of large roofs of stadiums and arena", *J. Wind Eng. Ind. Aerod.*, **95**(9-11), 871-887.
- Biagini, P., Borri C., Majowiecki, M., Orlando, M. and Procino, L. (2006), "BLWT tests and design loads on the roof of the new Olympic stadium in Piraeus", *J. Wind Eng. Ind. Aerod.*, **94**(5), 293-307.
- Bienkiewicz, B., Tamura, Y., Ham, H.J., Ueda, H. and Hibi, K. (1995), "Proper orthogonal decomposition and reconstruction of the multi-channel roof pressure", *J. Wind Eng. Ind. Aerod.*, **54-55**, 369-381.
- Chen, L. and Letchford, C.W. (2006), "Multi-scale correlation analyses of two lateral profiles of full-scale downburst wind speeds", *J. Wind Eng. Ind. Aerod.*, **94**(9), 675-696.
- Davenport, A.G. (1995), "How can we simplify and generalize wind loads?", *J. Wind Eng. Ind. Aerod.*, 54-55, 657-669.
- Endo, M., Bienkiewicz, B. and Ham, H.J. (2006), "Wind-tunnel investigation of point pressure on TTU test building", *J. Wind Eng. Ind. Aerod.*, **94**(7), 553-578.
- Fu, J.Y. and Li, Q.S. (2007), "Wind effects on the world's longest spatial latticed structure: loading characteristics and numerical prediction", *J. Constr. Steel Res.*, **63**(10), 1341-1350.
- GB50009-2001.(2002), *Load code for the design of building structures*, China Architecture & Building Press, Bei Jing (in Chinese).
- Holmes, J.D. (2001) , "Wind loading of structures", E & FN Spon, London.
- Holmes, J.D., Denoon, R.O., Kwok, K.C.S. and Glanville, M.J. (1997), "Wind loading and response of large stadium roofs", *Proceedings of the IASS International Symposium '97 on Shell and Spatial Structures*, Singapore, November.
- Jeary, A.P. (1997), "Designer's guide to the dynamic response of structures", E & FN Spon, London.
- Jeong, S.H., Bienkiewicz, B. and Ham, H.J. (2000), "Proper orthogonal decomposition of building wind pressure specified at non-uniformly distributed pressure taps", *J. Wind Eng. Ind. Aerod.*, **87**(1), 1-14.
- Levitan, M.L. and Mehta, K.C. (1992), "Texas tech field experiments for wind loads", *J. Wind Eng. Ind. Aerod.*, **43**(1-3), 1565-1588.
- Li, Q.S., Fang, J.Q., Jeary, A.P. and Wong, C.K. (1998), "Full scale measurements of wind effects on tall buildings", *J. Wind Eng. Ind. Aerod.*, **74-76**, 741-750.
- Li, Q.S., Fang, J.Q., Liu, D.K., Jeary, A.P. and Wong, C.K. (2000), " Evaluation of wind effects on a super tall building based on full scale measurements", *Earthq. Eng. Struct. D.*, **29**(12), 1845-1862.
- Li, Q.S. and Melbourne, W.H. (1996), "Pressure fluctuations on the Texas Tech Building model in various turbulent flows", *Proceedings of the Bluff Body Aerodynamics and Application, AIX9-AIX12*, Blacksburg, July.
- Li, Q.S., Xiao, Y.Q., Fu, J.Y. and Li, Z.N. (2007), "Full-scale measurements of wind effects on the Jin Mao building", *J. Wind Eng. Ind. Aerod.*, **95**(6), 445-466.
- Li, Q.S., Xiao, Y.Q., Wong, C.K. and Jeary, A.P. (2004), "Field measurements of typhoon on a super tall building", *Eng. Struct.*, **26**(2), 233-244.
- Melbourne, W.H. (1995), "The response of large roofs to wind action", *J. Wind Eng. Ind. Aerod.*, **54-55**, 325-336.
- Qu, W.L., Teng, J. Xiang, H.F., Zhong, L., Liu, H. Wang, J. and Li, G.B. (2006), "Intelligent health monitoring for roof space truss structures of the Shenzhen civic center under wind load", *J. Building Struct.*, **27**(1), 1-8 (in Chinese).
- Rocha, M.M., Cabral, S.V.S. and Riera, J.D. (2000), "A comparison of proper orthogonal decomposition and Monte Carlo simulation of wind pressure data", *J. Wind Eng. Ind. Aerod.*, **84**(3), 329-344.
- Stathopoulos, T., Marathe, R. and Wu, H. (1999), "Mean wind pressures on flat roof corners affected by

- parapets: field and wind tunnel studies”, *Eng. Struct.*, **21**(7), 629-638.
- Tamura, Y., Ueda, H., Kikuchi, H., Hibi K., Suganuma. S. and Bienkiewicz, B.(1995), “Proper orthogonal decomposition study of approach wind-building pressure correlation”, *Proceedings of the 9th International Comparison between Wind Load by Wind Tunnel Test and... 19 Conference on Wind Engineering*, New Delhi, India, January.
- Tubino, F. and Solari, G. (2007), “Gust buffeting of long span bridges: double modal transformation and effective turbulence”, *Eng. Struct.*, **29**(8), 1698-1707.
- Zhao, J.G. and Lam, K.M. (2002), “Characteristics of wind pressures on large cantilevered roofs: effect of roof inclination”, *J. Wind Eng. Ind. Aerod.*, **90**(12-15), 1867-1880.

CC